Open Access Journal

Journal of Power Technologies 96 (4) (2016) 295–305

journal homepage:papers.itc.pw.edu.pl

Model-based research on a micro cogeneration system with Stirling engine

Adrian Chmielewski*, Robert Gumiński, Jędrzej Mączak, Przemysław Szulim

Warsaw University of Technology, Faculty of Automotive and Construction Machinery Engineering, Institute of Vehicles, Narbutta 84, 02-524 Warsaw, Poland

Abstract

One of the elements and purposes of the climate-energy policy of the European Union is to increase the efficiency of conversion of the energy from fossil fuels. Managing high-temperature heat losses which accompany the technological processes, especially in thermal power engineering, serves this goal. An example of effective use of this heat is through the application of distributed generation devices (including: fuel cells, microturbines, and Stirling engines), which produce in combination electric energy, or mechanical energy and heat. This paper presents research into a micro cogeneration system with a Stirling engine, using nitrogen as a working gas. A crucial element of the research is model-based analysis of changes in selected thermodynamic parameters, including among others: pressure change in the working cylinder. The presented comparison of the research results, as well as the results of simulation, effectively support the prediction processes as regards the system.

Keywords: Stirling engine; micro cogeneration system; energy; thermodynamic processes; simulation

1. Introduction

The 2030 perspective [1–3] sets goals for the member states of the European Union with respect to energy. These purposes include: increasing power efficiency to 27%, growth of renewables [1, 2] in the energy market to 27%, and reduction of CO_2 emissions by nearly 40% [1–3]. Improved energy efficiency is perceived as dependent on the development of distributed generation [4–7]. In many sources of distributed generation [4, 6] changing the form of chemical energy (e.g.: fuel energy—internal combustion engines or energy of working element, for example Stirling engines [8–18]) into mechanical energy takes place with the use of various working mechanisms (among others: the piston-crankshaft mechanism, rhombic drive mechanism, the mechanism with an oblique disk, and other combined mechanisms). The most frequently used transmission mechanism in engine construction practice is the piston-crankshaft assembly [19–21].

This paper presents geometric, analytical and simulation models of the piston camshaft mechanism with three degrees of freedom in the Alpha-type Stirling engine. A dynamic model has been connected with the isothermal submodel of the heat exchange in the working space (Fig. 8). It should also be mentioned that similar works were conducted by the authors [12, 14, 17–20]. In work [12], a dynamic model of the Stirling engine was presented, the key element of which was a piston-crankshaft assembly. A model of changing dynamics of the piston-crankshaft assembly was connected with a thermodynamic second-order model, which takes into account energy and heat losses taking place in the engine [12].

As was mentioned in the context of the growing interest in cogeneration systems and distributed micro cogeneration [4], which comprises among others Stirling engines [8–18, 21–44], the need arises to optimize (improve efficiency) and rationalize management of waste heat. It is thus worthwhile preparing tasks related to optimization of the parameters of the Stirling engine work [24–31]. A dynamic model of the Stirling engine, presented in this work, will be used to serve this purpose.

The prepared model of the piston-crankshaft assembly will be extended in the future with subsequent constituent parts, among others: a quasi-adiabatic model of heat exchange [32, 33] during operation of the heat cycle with the purpose of providing a faithful description of processes taking place in a real engine, and an optimization model [22–31] of the geometric parameters (depending on the needs, the purpose can be maximum overall efficiency, utility power, or minimum entropy increase in the course of the heat exchange processes). Depending on the input parameters, a multi-layer neural network [34] or Fuzzy Logic [37] will as-

*Corresponding author

Email address: a.chmielewski@mechatronika.net.pl (Adrian Chmielewski)

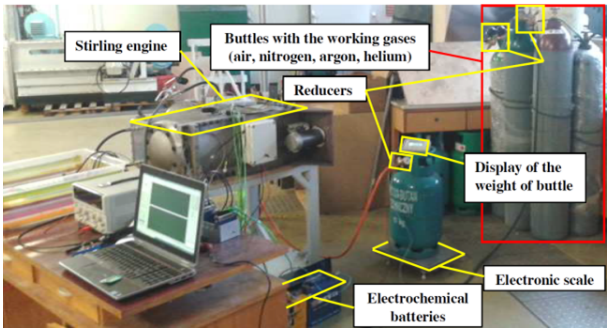

Figure 1: Testing workbench [8–10]

sure the adaptiveness of the model's work.

Such an approach will make it possible to investigate the influence of the chosen work parameters and their optimization in order to obtain maximum efficiency and to use this knowledge on a real object.

In this work, differential equations are presented, describing the dynamic model of the piston-crankshaft system. These equations are coupled with differential equations describing the isothermal heat exchange in the working space. The precursors of mathematical description of the isothermal heat exchange in the working space were Urieli and Berchowitz [22, 25], and Walter [24], as well as Organ [42] and Shoureshi [23]. In Poland, the precursor of mathematical modelling of the thermodynamic processes in the Stirling engine was Zmudzki [43]. Unfortunately, their models did not take into consideration the dynamics of the piston-crankshaft assembly, which has a huge significance in transient states, for example during startup of the Stirling engine [21].

In the present work, on the basis of the energy balance in the control spaces, the change of control parameters was simulated: parameters such as theoretical work, theoretical power, and flow of the working gas mass in the chosen inspection points (expansion space–heater, heater–regenerator, regenerator–cooler, cooler–compression space). The simulation results of the change in cylinder pressure were validated against test bench research.

2. Description of the test bench

The laboratory workbench where the tests were conducted consisted of a single-action Alpha-type Stirling engine (Fig. 1), a belt transmission with an $i = 1 : 4$ ratio between the Stirling engine and the electric DC engine (electric engine rated power—500 W), the gauging sensors (pressure converter placed in the cold cylinder, magneto-inductive sensor) of gauging thermocouples—Fig. 2 (of the K-type, located in: the compression space (V_c), with temperature T_c, expansion space (V_e), with temperature T_e, and on the regenerator (R) from the side of the cooler with temperature T_{rc}, as well as from the heater side, with temperature T_{rh}), a loading system for up to 550 watts (the loading system

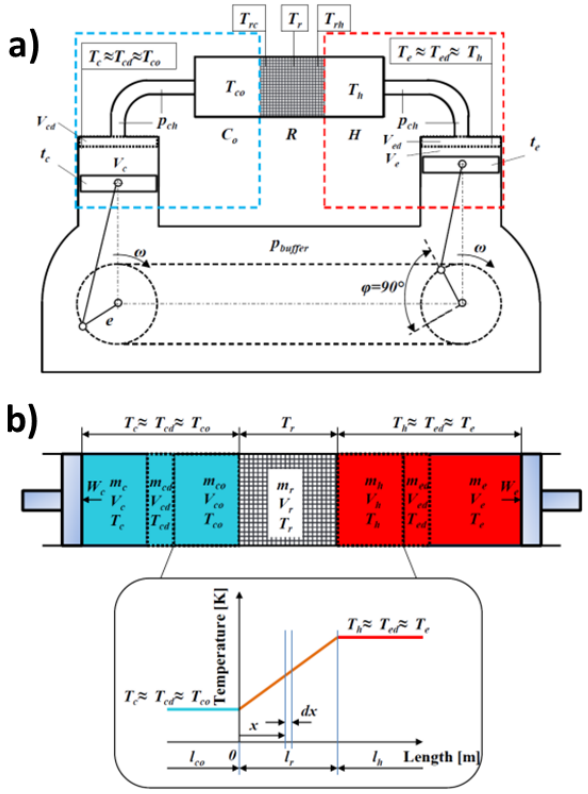

Figure 2: Diagram of a real-life Stirling engine and illustration of temperature change in working space [8]

worked as an adjustable current source), National Instruments cards, and Labview software to register the chosen parameters. For startup of the micro cogeneration system with the Stirling engine, 2 serially connected lead-acid 12 V batteries (Forse 55 Ah) were used.

The working gas, nitrogen in this case, was delivered from a pressure container (Fig. 1) to the buffer space p_{buffer}, and to the working space p_{ch}. During the tests, the temperatures in compression space T_{Co}, expansion space T_e, on the regenerator from the cold side T_{rc} and the hot side T_{rh} (Fig. 2a) were registered in parallel, as were the rotational velocity of the Stirling engine (which was converted to the velocity of the electric motor at the known ratio between the electric motor and the Stirling engine), the current fed to the loading system, the voltage on the electric motor, and the pressure in the cold cylinder (the compression space). Fig. 2 shows a diagram of the Stirling engine construction (Fig. 2a), as well as an illustration of the temperature changes in the working space (Fig. 2b).

The angular shift between the piston working in the compression space (t_c) and the piston working in the expansion space (t_e) was $90°$. Fig. 2a illustrates temperature change in the working space. It was assumed that the temperature of the lower heat source is approximately equal to the temperature in the compression space, in the dead space above the piston, and in the cooler space, which means that $T_c \approx T_{cd} \approx T_{co}$. A similar simplification was adopted for the upper heat source. It was assumed that the temperatures in

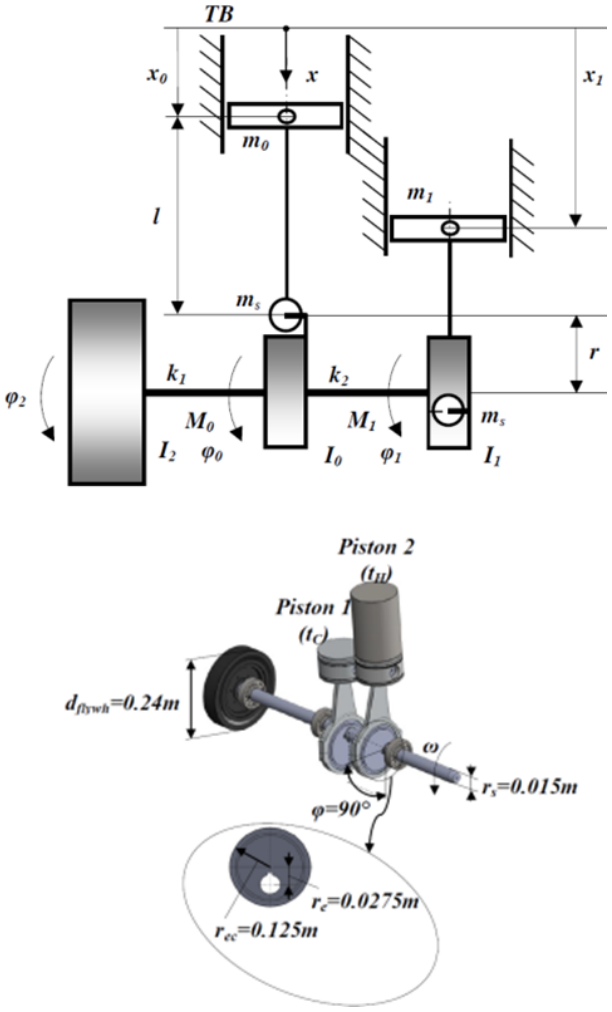

Figure 3: Model of the piston-crankshaft assembly [21]

the expansion space V_e, in the dead space above the piston V_{ed} working in the expansion space and in the heater space V_h are roughly the same, which means that $T_h \approx T_{ed} \approx T_e$. It is a known fact that temperature T_r on the l_r regenerator length ranges between the temperature of the lower T_c and upper T_h heat source (it is a linear relationship in approximation). In order to determine the temperature on the regenerator, relationships from (14) to (16) were used, aspresented in subchapter 2.1.

2.1. Dynamic model of the piston-crankshaft assembly and the model of isothermal heat exchange—theoretical considerations

The model presented in this work concerns the piston-crankshaft assembly used in, among others, Stirling engines. The geometry of the presented piston-crankshaft assembly is different from the geometry of the piston-crankshaft assembly of the combustion engine due to the fact that the cranks in the two-cylinder combustion engine's layout are offset by $180°$ against each other, whereas in the discussed system the angle between cranks of the hot and cold cylinders is $90°$. Fig. 3 shows the geometric model, which assumes static reduction of the connecting rod masses.

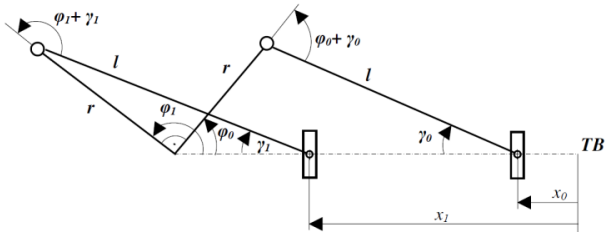

Figure 4: Diagram illustrating geometry of the considered piston-crankshaft assembly [21]

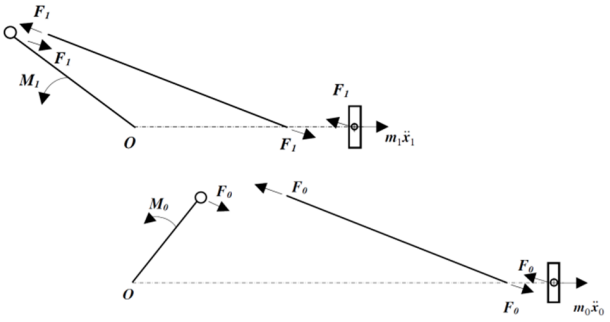

Figure 5: Diagram showing the distribution of forces in the considered system [21]

Similar assumptions were made in works [19–21]. The analyzed physical model has three degrees of freedom. The flywheel is connected with the shaft by means of the elastic element of the k_1 rigidity (section: flywheel—the first piston). On the farther section between the first and the second piston, the shaft has rigidity k_2.

The crank of piston 1 (Fig. 3) is shifted against the crank of piston 2 by the angle of $90°$. Fig. 4 shows a diagram of the crankshaft mechanism with the angles marked, which will serve the purpose of determining the equations of motion.

From analysis of Fig. 3, 4 and 5, the equation of moments can be written for crank 2 inertia:

$$\begin{aligned} I_1\ddot{\varphi}_1 = M_1 - F_1 r \sin(\varphi_1 + \gamma_1 + 90°) \\ -k_1(\varphi_1 - \varphi_0) \end{aligned} \tag{1}$$

The crank 1 motion can be described with a similar equation:

$$\begin{aligned} I_0\ddot{\varphi}_0 = M_0 - F_0 r \sin(\varphi_0 + \gamma_0) \\ -k_2(\varphi_0 - \varphi_2) + k_1(\varphi_1 - \varphi_0) \end{aligned} \tag{2}$$

The sum of moments for the flywheel (Fig. 1) is:

$$I_2\ddot{\varphi}_2 = k_2(\varphi_0 - \varphi_2) \tag{3}$$

The sum of projections of the forces on the x-axis for piston 2 (on the basis of Fig. 4) is:

$$F_1 \cos\gamma_1 - m_1\ddot{x}_1 = 0 \tag{4}$$

The sum of projections of the forces on the x-axis for piston 1 (on the basis of Fig. 4) is:

$$F_0 \cos\gamma_0 - m_0\ddot{x}_0 = 0 \tag{5}$$

From the trigonometric dependencies (the theorem of sinuses) the relations can be determined (relations between γ_0 and φ_0 and also γ_1 and φ_1. The detailed derivation path for these dependencies was shown in work [21].

The last unknown for determining forces F_0 and F_1 from equations (4) and (5) are the linear accelerations $\ddot{x}_0$ and $\ddot{x}_1$. In order to define the sought unknown on the basis of analysis of the kinematic relationships shown in Fig. 4, employing the theorem of sinuses allows for eliminating the angle γ_0, then:

$$x_0(\varphi_0) = r\left\{(1-\cos\varphi_0) + \frac{l}{r}(1-\sqrt{1-\frac{r^2}{l^2}\sin^2\varphi_0})\right\} \quad (6)$$

Expanding the root from (6) into a power series, which was limited to the first two terms, the final relationship for x_0 can be formulated:

$$x_0(\varphi_0) = r\left\{(1-\cos\varphi_0) + \frac{\lambda}{4}(1-\cos 2\varphi_0)\right\} \quad (7)$$

As a result of differentiating the equation (7), a relationship describing linear velocity and linear acceleration for piston 1 (t_C) is obtained. The detailed derivation of the relationship of the piston 1 velocity and acceleration was presented in work [21].

According to the assumptions made, the linear displacement for piston 2 (t_H) is offset against piston 1 (t_C) by the value corresponding to the difference of crank angles amounting to 90°, which can be described by the following:

$$\begin{gathered} x_1(the\varphi_1 + 90^\circ) = \\ r\left[(1-\cos(\varphi_1+90^\circ)) + \frac{\lambda}{4}(1-\cos(2\varphi_1+180^\circ))\right] \end{gathered} \quad (8)$$

Using the trigonometric relationships (reduction formulae), the expression (8) was reduced to the form of:

$$x_1 = r\left\{(1+\sin(\varphi_1)) + \frac{\lambda}{4}(1+\cos(2\varphi_1))\right\} \quad (9)$$

As a result of differentiating the equation (9) the relationship is obtained, describing linear velocity and linear acceleration for piston 2. The detailed derivation of these relationships was presented in work [21].

The moment acting on the piston 1 shaft (t_C) can be described with an equation which takes into consideration the change of pressure in a cylinder, acting on the bottom; this can be written as follows:

$$M_0 = pA_C x_0 \quad (10)$$

The moment acting on the piston 2 shaft (t_H) can be described with an equation which takes into consideration the change of pressure in a cylinder, acting on the bottom; this can be written as follows:

$$M_1 = pA_H x_1 \quad (11)$$

Based on the real object, the assumption was made that $A_c = A_e = A$, and it was assumed that $M_0 = M_1$ with respect to the value.

Pressure p in the working space was approximated as a mean pressure, which can be determined on the basis of the known total mass of the gas in the working space [22–24, 42, 43]. The total mass of gas in the working space is a sum of masses in individual working spaces, which can be described by the relationship:

$$m_{tot} = m_c + m_{cd} + m_{co} + m_r + m_h + m_{ed} + m_e \quad (12)$$

On the basis of the Clapeyron equation $pV = mRT$ for individual working spaces, the relationship describing the working gas mass in the working space can be written, taking into account the thermodynamic parameters of the gas in each of the spaces, with the assumption that the mean pressure in the working chamber is constant:

$$m_{tot} = \frac{p}{R}\left(\frac{V_c}{T_c} + \frac{V_{cd}}{T_{cd}} + \frac{V_{co}}{T_{co}} + \frac{V_r}{T_r} + \frac{V_h}{T_h} + \frac{V_{ed}}{T_{ed}} + \frac{V_e}{T_e}\right) \quad (13)$$

In relationship (13) the temperature on the regenerator's element T_r changes along its length, which can be written as follows:

$$T_r(x) = x(T_h - T_c)/l_r + T_c \quad (14)$$

Analysing Fig. 2 leads to the conclusion that if the relationship (14) describing temperature change is inserted in the Clapeyron equation, then we receive [22, 25]:

$$\begin{gathered} m_r = \frac{A_r l_r}{R}\int_0^{l_r} p\frac{1}{(T_h-T_c)x+T_c l_r}dx = \\ p\frac{V_r}{R(T_h-T_c)}\ln\frac{T_h}{T_c} \end{gathered} \quad (15)$$

As a consequence, the temperature on the regenerator can be determined, and it is:

$$T_r = \frac{T_h - T_c}{\ln\frac{T_h}{T_c}} \quad (16)$$

Transforming relationship (13), and inserting (16) into it, the relationship describing pressure change in the working space can be formulated:

$$p = \frac{m_{tot}R}{\frac{V_c}{T_c} + \frac{V_{cd}}{T_{cd}} + \frac{V_{co}}{T_{co}} + \frac{V_r}{T_r} + \frac{V_h}{T_h} + \frac{V_{ed}}{T_{ed}} + \frac{V_e}{T_e}} \quad (17)$$

It should be emphasised here that with respect to modelling the pressure changes in the working space, the dead volume values of heat exchangers are essential. They directly influence the amplitude value of pressure changes in the working space [24].

The volume change V_{Co} in the compression space using the relationship describing x_0 (7) can be written in the following way:

$$V_c = x_0(\varphi_0)A_c \quad (18)$$

The change of volume V_e in the compression space using the relationship describing x_1 (9) can be written as follows:

$$V_e = x_1(\varphi_0)A_e \quad (19)$$

The total dead volume present in the considered system can be written as follows:

$$V_{dead} = V_{co} + V_{cd} + V_r + V_h + V_{ed} \tag{20}$$

The total change of volume in the working space can be written as follows:

$$V_{all} = V_{dead} + V_c + V_e \tag{21}$$

The work performed by the gas in compression and expansion spaces can be formulated as follows:

$$L_{teor} = \oint pdV_{comp} + \oint pdV_{exp} = \oint p\frac{dV_{comp}}{d\varphi}d\varphi + \oint p\frac{dV_{exp}}{d\varphi}d\varphi \tag{22}$$

With $dV_e/d\varphi$ being:

$$\frac{dV_e}{d\varphi} = A_e\frac{dx_1}{d\varphi_1} \tag{23}$$

With $dV_c/d\varphi$ being:

$$\frac{dV_c}{d\varphi} = A_c\frac{dx_0}{d\varphi_0} \tag{24}$$

The flow of the working gas mass in individual sections of the working space can be determined by means of the equations:

$$\dot{m}_i = \frac{dmi}{dt} = \frac{d}{dt}\left(\frac{p_iV_i}{RT_i}\right) = \frac{dp_i}{dt}\frac{V_i}{RT_i} + \frac{dV_i}{dt}\frac{p_i}{RT_i} \tag{25}$$

The theoretical power rendered by the gas for a single working cycle can be written as:

$$P = \frac{\omega_i}{2\pi}L_{teor} = f_iL_{teor} \tag{26}$$

The theoretical power rendered by the gas for the considered simulation time can also be written as:

$$P_{teor} = \frac{L_{teor}}{t_{sim}} \tag{27}$$

From relationship (17), $\dot{p}_i$ can be determined:

$$\dot{p} = \frac{dp}{dt} = \frac{d}{dt}\left(\frac{m_{tot}R}{\frac{V_c}{T_c} + \frac{V_{cd}}{T_{cd}} + \frac{V_{co}}{T_{co}} + \frac{V_r}{T_r} + \frac{V_h}{T_h} + \frac{V_{ed}}{T_{ed}} + \frac{V_e}{T_e}}\right) \tag{28}$$

Fig. 6 presents the space of heat exchange.
The equation of state for a system considered in this way (Fig. 6) can be written as follows:

$$dQ + c_pT_{inp}\frac{dm_{inp}}{dt} - c_pT_{out}\frac{dm_{out}}{dt} = dL_{teor} + c_v\frac{d}{dt}(mT) \tag{29}$$

For isothermal transformations $T_{inp} = T_{out} = T = \text{const}$ and $\frac{dm_{inp}}{dt} - \frac{dm_{out}}{dt} = \frac{dm}{dt}$ can be written consequently as:

$$dQ + c_pT\frac{dm}{dt} = dL_{teor} + c_vT\frac{dm}{dt} \tag{30}$$

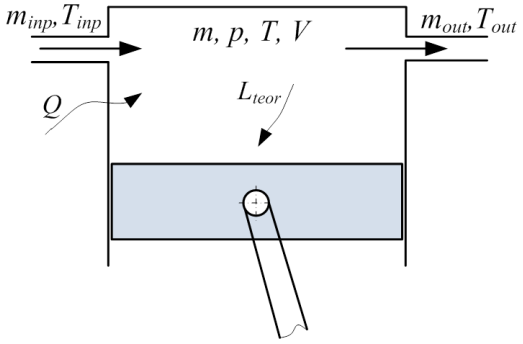

Figure 6: Considered space of energy exchange

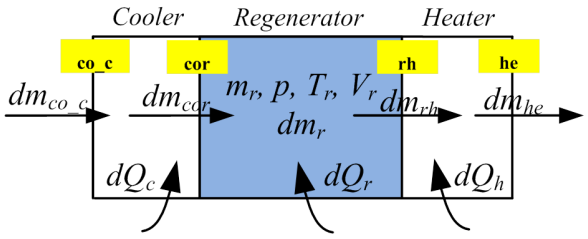

Figure 7: Mass flow and heat exchange on heat exchangers (isothermal process)

As a consequence, the following can be written for the heat exchangers, knowing that $dV_i = dV_{comp} + dV_{exp}$:

$$\begin{aligned} dQ &= dL_{teor} + T\frac{dm}{dt}\left(c_v - c_p\right) = p\left(dV_{comp} + dV_{exp}\right) \\ -RT\frac{dm}{dt} &= -RT\frac{1}{RT}\left(\frac{dp}{dt}V_i + \frac{dV_i}{dt}p\right) + pdV_i = -\frac{dp}{dt}V_i \end{aligned} \tag{31}$$

For the cooler $V_i = V_c$:

$$dQ_c = -\frac{dp}{dt}V_c \tag{32}$$

For the heater $V_i = V_h$:

$$dQ_h = -\frac{dp}{dt}V_h \tag{33}$$

Fig. 7 shows a schematic flow of working gas mass and heat exchange taking place on the cooler, regenerator, and heater.
For the regenerator, where the cyclical cooling and heating of the working gas takes place $dL_{teor} = 0$. Therefore, the energy balance can be written as follows:

$$dQ_r + c_pT_c\frac{dm_c}{dt} - c_pT_h\frac{dm_h}{dt} = c_vT\left(\frac{dp}{dt}V_i + \frac{dV_i}{dt}p\right)\frac{1}{RT} \tag{34}$$

Transforming the above we obtain:

$$dQ_r = -c_p\left(T_c\frac{dm_c}{dt} - T_h\frac{dm_h}{dt}\right) + c_v\left(\frac{dp}{dt}V_r + \frac{dV_r}{dt}p\right)\frac{1}{R} \tag{35}$$

For the regenerator $V_i = V_r = \text{const}$:

$$\begin{aligned} dQ_r = -c_p\left(T_c\frac{dm_c}{dt} - T_h\frac{dm_h}{dt}\right) + c_vV_r\frac{dp}{dt}\frac{1}{R} = \\ c_vV_r\frac{dp}{dt}\frac{1}{R} - c_p\left(T_c\frac{dm_c}{dt} - T_h\frac{dm_h}{dt}\right) \end{aligned} \tag{36}$$

Knowing that the temperature at the boundaries of the range for $x = 0$ and for $x = l_r$ is, respectively T_c and T_h (Fig. 2b), we can write the following:

$$\frac{dm_c}{dt} = \frac{dp}{dt}\frac{V_c}{RT_c} + \frac{dV_c}{dt}\frac{p}{RT_c} \tag{37}$$

and

$$\frac{dm_h}{dt} = \frac{dp}{dt}\frac{V_h}{RT_h} + \frac{dV_h}{dt}\frac{p_i}{RT_h} \tag{38}$$

It was assumed that during the working cycle the mass of the working gas is pushed from the cold side, which can be written for the control boundary cor:

$$\begin{gathered}\frac{dm_{cor}}{dt} = -\frac{dm_c}{dt} - \frac{dm_{cd}}{dt} - \frac{dm_{co}}{dt} = \\ -\frac{1}{RT_c}\left[\frac{dp}{dt}(V_c + V_{cd} + V_{co}) + p\frac{dV_c}{dt}\right]\end{gathered} \tag{39}$$

Additionally, the assumption has been made that during the working cycle the mass of the working gas is pushed from the regenerator to the hot side, which can be written for the control boundary rh:

$$\begin{gathered}\frac{dm_{rh}}{dt} = \frac{dm_h}{dt} + \frac{dm_{ed}}{dt} + \frac{dm_e}{dt} = \\ \frac{1}{RT_h}\left[\frac{dp}{dt}(V_h + V_{ed} + V_e) + p\frac{dV_e}{dt}\right]\end{gathered} \tag{40}$$

As a consequence we can write:

$$\begin{gathered}dQ_r = -c_p\left(T_c\frac{dm_{cor}}{dt} - T_h\frac{dm_{rh}}{dt}\right) + c_v V_r\frac{dp}{dt}\frac{1}{R} = c_v V_r\frac{dp}{dt}\frac{1}{R} + \ldots \\ -c_p\left(-T_c\frac{1}{RT_c}\left[\frac{dp}{dt}(V_c + V_{cd} + V_{co}) + p\frac{dV_c}{dt}\right] + \right. \\ \left. -T_h\frac{1}{RT_h}\left[\frac{dp}{dt}(V_h + V_{ed} + V_e) + p\frac{dV_e}{dt}\right]\right)\end{gathered} \tag{41}$$

Transforming (41) we obtain the ultimate form of the relationship describing the heat exchange taking place on the regenerator:

$$\begin{gathered}dQ_r = -c_p\left(T_c\frac{dm_{cor}}{dt} - T_h\frac{dm_{rh}}{dt}\right) + c_v V_r\frac{dp}{dt}\frac{1}{R} = c_v V_r\frac{dp}{dt}\frac{1}{R} + \ldots \\ +c_p\frac{1}{R}\left(\left[\frac{dp}{dt}(V_c + V_{cd} + V_{co} + V_h + V_{ed} + V_e) + p\left(\frac{dV_c}{dt} + \frac{dV_e}{dt}\right)\right]\right)\end{gathered} \tag{42}$$

Using the relationship (12) and assuming that $m_{tot} = \text{const}$, after two-sided differentiation, we obtain:

$$0 = dm_c + dm_{cd} + dm_{co} + dm_r + dm_h + dm_{ed} + dm_e \tag{43}$$

For the boundary line the cold cylinder–cooler $(co - c)$, the following can be written:

$$\begin{gathered}dm_{co-c} = -dm_c - dm_{cd} \Rightarrow \frac{dm_{co-c}}{dt} = -\frac{V_c}{RT_c}\frac{dp}{dt} \\ +p\frac{1}{RT_c}\frac{dV_c}{dt} - V_{cd}\frac{1}{RT_c}\frac{dp}{dt} = \frac{1}{RT_c}\left[p\frac{dV_c}{dt} - \frac{dp}{dt}(V_c + V_{cd})\right]\end{gathered} \tag{44}$$

For the boundary zone $(co - r)$, the following can be written:

$$\begin{gathered}dm_{cor} = dm_{co-c} - dm_{co} = dm_{co-c} \\ -V_{co}\frac{1}{RT_c}\frac{dp}{dt} = \frac{1}{RT_c}\left[p\frac{dV_c}{dt} - \frac{dp}{dt}(V_c + V_{cd} + V_{co})\right]\end{gathered} \tag{45}$$

For the boundary zone $(r - h)$ the following can be written:

$$dm_{rh} = dm_{he} + dm_h = \frac{1}{RT_h}\left[p\frac{dV_e}{dt} + \frac{dp}{dt}(V_e + V_{ed} + V_h)\right] \tag{46}$$

For the boundary zone $(h - e)$ the following can be written:

$$dm_{he} = dm_e + dm_{ed} = \frac{1}{RT_h}\left[p\frac{dV_e}{dt} + \frac{dp}{dt}(V_e + V_{ed})\right] \tag{47}$$

As a consequence, for the change of mass dm_r the following can be written:

$$dm_r = dm_{rh} - dm_{rc} \tag{48}$$

3. Simulation model of the system

On the basis of the given relationships (1–48) a simulation model was built (Fig. 8), describing the dynamics of the piston-crankshaft assembly with three degrees of freedom, as well as an isothermal thermodynamic model of heat exchange in the working space.

Table 1 shows input parameters for the simulation model (Fig. 4) based on the real Stirling engine.

3.1. Simulation and workbench test results

Fig. 9 shows a closed-loop diagram of pressure changes (Fig. 9a), and an open diagram (Fig. 9b). The change in pressure relative to the mean pressure for nitrogen $p = 0.45$ MPa is ± 0.13 MPa. The indicator closed-loop diagrams originating from the tests and the model are similar. Fig. 9b presents an open diagram, a curve obtained in the course of the workbench tests. The amplitude of oscillations for the open diagram of the pressure resulting from the tests is similar to that obtained from the model (Fig. 15b) in the fixed states.

Fig. 10 presents curves p(V) of volume changes of the working space V_c of the cold piston (t_c), V_e of the hot piston (t_h) and the sum of their total volume (V_{all}) in the course of the working cycle, derived from the simulation model. Similar results with change of pressure were obtained from the tests, which were presented in work [8]. Fig. 10 shows that the mean pressure of the working gas increases with the rising temperature of the upper heat source.

As follows from the analysis of the influence of the upper heat source temperature originating from the research (Fig. 11), with the growing difference of the temperature values ($T_c = \text{const}$ and temperature growth T_e) the electric power value increases. For nitrogen, with $p = 0.5$ MPa, with changing temperature from $T_e = 780$ K to $T_e = 910$ K, there is a nearly 10 W increase in electric power.

Fig. 12 presents the influence of pressure change on the value of the μCHP system electric power. In the case of nitrogen, for the pressure value $p = 0.3$ MPa, the value of maximum power was 19.77 W at $n = 412.25$ revs/min. Analyzing the curves shown in Fig. 12 it can be seen that the increase in pressure from 0.3 to 0.5 MPa is accompanied by an increase in rotational velocity. For $p = 0.4$ MPa and $T_e = 910$ K, the electric power was 41.5 W with $n = 546.7$ revs/min.

Fig. 13 illustrates the influence of the upper heat source temperature on theoretical work L_{teor}, and the increase in theoretical work δL_{teor}. Theoretical work increases as a function of crankshaft rotation. Analysis of Fig. 13a shows that work increases more rapidly with the increasing difference in temperatures (increase of T_e with $T_c = \text{const}$). The highest amplitude among the considered cases, of the theoretical work increase, occurs for $T_e = 910$ K and is 43 J/rotation (-18.1;+24.3) of the crankshaft $(360°)$.

Fig. 14 illustrates the influence of the upper heat source temperature on theoretical power value. With the growing temperature of the upper heat source (T_h) the value of the theoretical power goes up, for $T_h = 910$ K theoretical power is

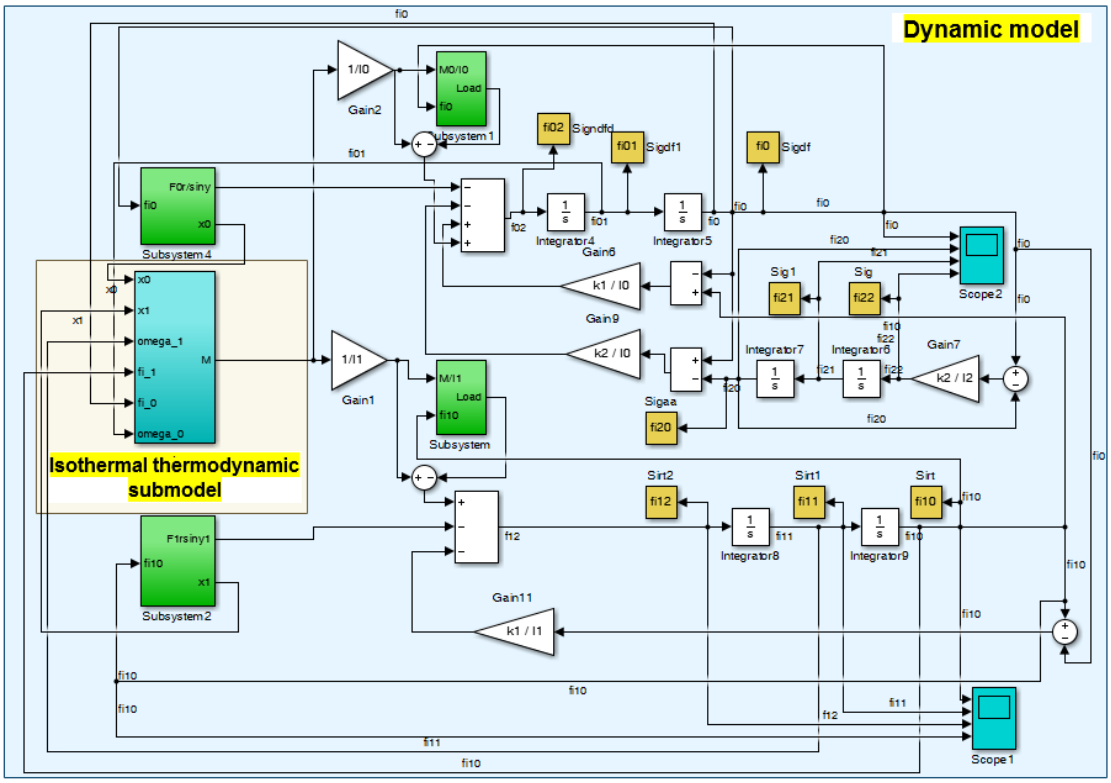

Figure 8: Simulation model designed with Matlab&Simulink

Table 1: Model input data

Parameter	Value	Parameter	Value
Individual gas constant for nitrogen	R_{N2}=296.95 J/kgK	Crankshaft radius	r_s=0.015 m
Temperature in compression space	T_c=301 K	Crankshaft mass	m_s=3.45 kg
Temperature in expansion space	T_{Ex}=910 K	Crank radius	r_{ec}=0.125 m
Total mass of working gas	m_{tot}=0.0055 kg	Crankshaft rigidity	$k_1 \approx k_2$=7200 Nm/rad
Volume of space V_{ed} (above piston t_C)	V_{cd}=0.00003 m^3	Piston diameter	D=0.11 m
Volume of cooler space V_{co}	V_{co}=0.00031 m^3	Regenerator length	l_r=0.055 m
Volume of space V_{ed} (above piston t_H)	V_{ed}=0.000044 m^3	Crankshaft length	D_{shaft}=0.8 m
Volume of heater space V_h	V_h=0.00029 m^3	Piston stroke $s = 2r$	s=0.055 m
Volume of regenerator space V_r	V_r=0.00022 m^3	Length of connecting rod	l=0.207 m
Reduced moment of crankshaft inertia for piston 1 (t_C)	I_0=0.0107 kgm^2	Mass of connecting rod	m_c=0.55 kg
Reduced moment of crankshaft inertia for piston 2 (t_H)	I_1=0.0132 kgm^2	Mass of piston 1	m_0=0.65 kg
Moment of flywheel inertia	I_2=0.024 kgm^2	Mass of piston 2	m_1=0.95 kg
Crankshaft length	l_s=0.8 m	Crankshaft rigidity	$k_1 \approx k_2$=7200 Nm/rad

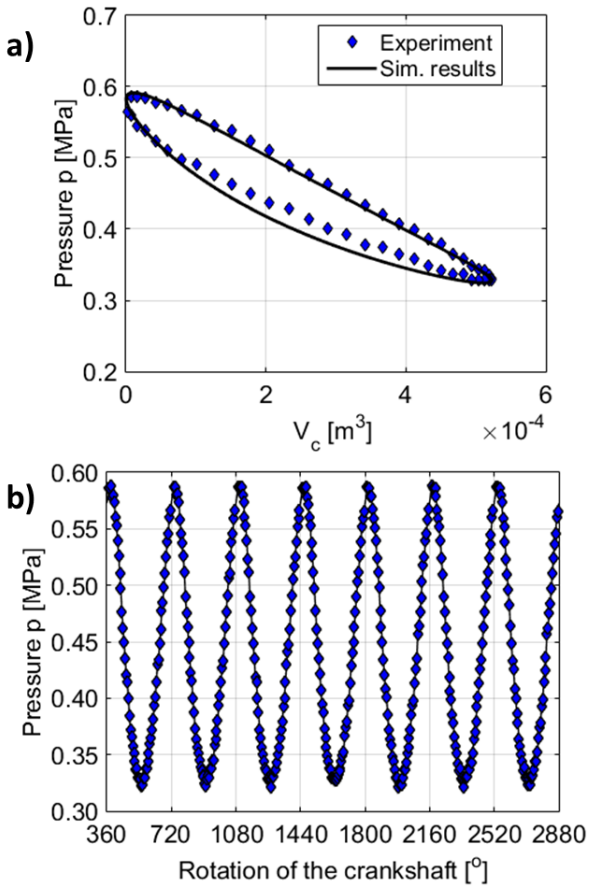

Figure 9: Closed loop diagram of pressure changes—comparison of results obtained from the model and tests a), curve of pressure changes—obtained from tests b)

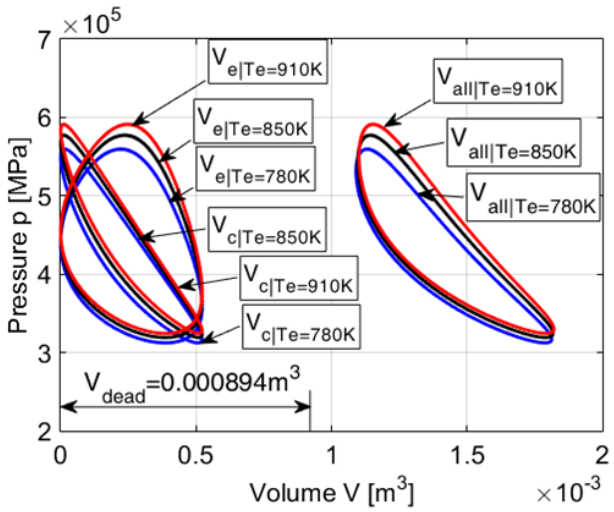

Figure 10: Influence of upper heat source temperature on the p(V) curve

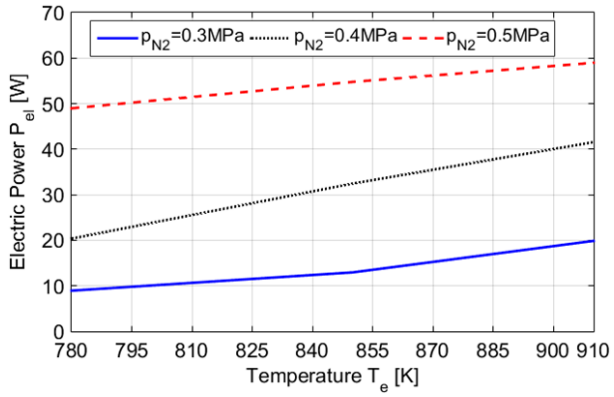

Figure 11: Influence of upper heat source temperature on the value of power of the μCHP

13.5 kW (up 2.12 kW relative to the temperature $T_h = 780$ K). It should be emphasised that curves obtained from the model do not take into consideration the losses occurring on the real object. The present results obtained from the simulation model should be seen as pointers in conjunction with the tests conducted simultaneously.

Fig. 15a illustrates the volume change in the compression space (V_c), expansion space (V_e), the sum of these spaces (V_e+V_c), as well as the change of the total volume in the working space (V_{all}), which also considers the sum of dead volumes V_{dead}. Fig. 15b presents the change in pressure simulated in the fixed state (when the mean angular velocity is fixed—Fig. 17b). The character of changes in the simulated pressure approximates the values obtained from the tests (Fig. 9b).

Fig. 16 illustrates the flow of the working gas mass through the control volumes. The results presented below were obtained by means of implementing relationships (1–48) into the model, and particularly the relationships (43–48), which describe the flow of the working gas mass at the control line. The greatest flows of the working gas mass occur at the border line cr where the gas (dm_{cr}) flows from the cooler to the regenerator. The character of changes dm_{cr} approaches sinusoidal. The lowest flow of the working gas mass occurs at the border line he (the expansion space–heater—Fig. 7) where the dm_{eh} flows. When analyzing the single work cycle (Fig. 16), attention should be paid to the mutual shift in the flow of the working gas masses. This is caused by the angular shift, which takes place in the real engine, as well as by the quantities of dead spaces, which qualitatively and quantitatively influence the character of the working gas flow. The greater the dead volume of the heat exchangers, the lower the amplitudes of changes of both: the theoretical work increase (Fig. 13) and the mass flow through the heat exchangers. In the case of the regenerator, the porous character of the element plays the key role, it usually ranges from 70 to 95% [42, 44].

In the dynamic model, the thermodynamic processes are accompanied by the phenomena occurring and resulting from the dynamics of the considered system. Fig. 17a shows the flow charts of angular displacements respectively for: crank 2 (φ_0), crank 1 (φ_1), and the flywheel (φ_2). Fig. 17b presents the flow charts of angular velocities, which are very similar in their character of changes (after 1s of simulation); angular velocity reaches values of: $\omega_0 = 1279$ rad/s (ampli-

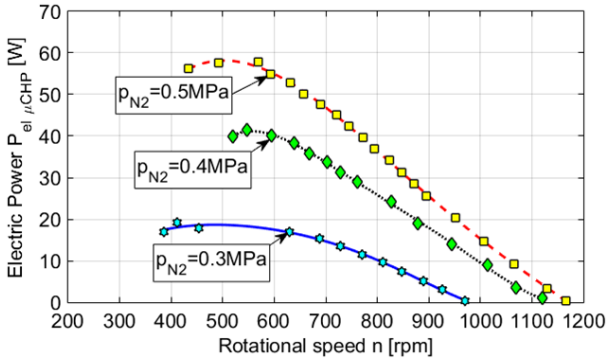

Figure 12: Influence of pressure change on the value of the μCHP system electric power

tude of oscillations is 228 rad/s), $\omega_1 = 1293.5$ rad/s (amplitude of oscillations is 153 rad/s), $\omega_2 = 1280$ rad/s (amplitude of oscillations is 38 rad/s) for the crankshaft-piston assembly discussed in this work.

Amplitude of angular velocity changes depends on the crankshaft's geometric dimensions, crankshaft rigidity, moments of inertia of individual elements of the piston-crankshaft system, as well as the character and value of forces acting on the bottom of pistons originating from the pressure changes in the compression and expansion spaces.

Work [21] also discusses the influence of different parameters on the dynamics of the piston-crankshaft assembly, such as: loading torque, moment of inertia of the flywheel, extortion torque, as well as the influence of the changing rigidity of the crankshaft on the values of displacement, velocity, angular acceleration and displacement, the values of piston velocity and acceleration.

4. Conclusions

This work presents theoretical considerations of the isothermal heat exchange in the working space of the Stirling engine. Analytical and simulation models of the piston-crankshaft assembly are presented, and selected results of the simulation of the piston-crankshaft assembly with three degrees of freedom are discussed. The dynamic model of the piston-crankshaft assembly was coupled with the thermodynamic model, which describes the isothermal heat exchange in the working space of the considered Stirling engine. The work presents the curves of dynamic parameters such as angular acceleration and angular velocity, theoretical work, theoretical power, and analysis of changes in those parameters made after the system determined an angular velocity. These included, among others: the curve of pressure in the working space, the flow of mass in the selected control volumes and changes in the control volumes as a function of the crankshaft's angle of rotation.

The pressure change in the cold cylinder (V_c) was compared with the test results. Also shown are the influence of the upper heat source temperature on the theoretical

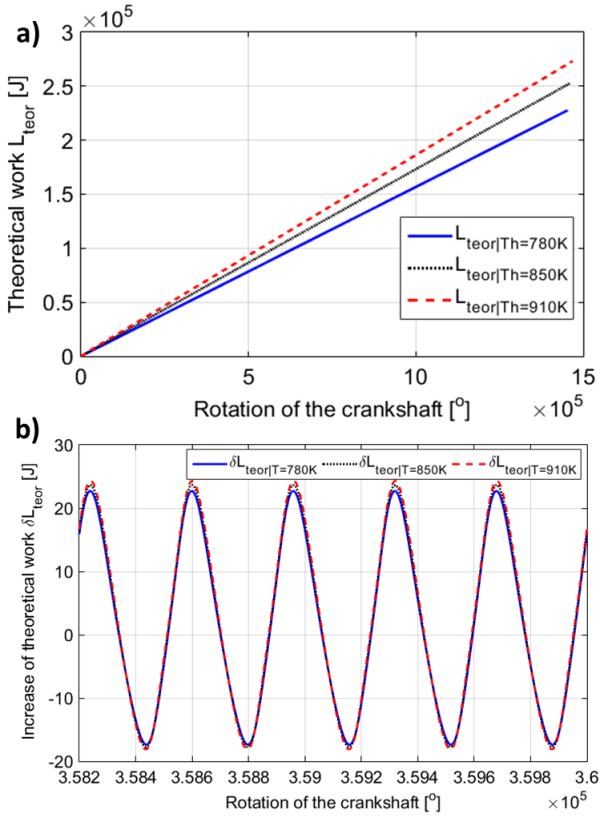

Figure 13: Influence of upper heat source temperature on: theoretical work L_{teror} a), increase in theoretical work δL_{teor} b)

closed diagram $p(V)$, and the increase in theoretical work and power. The simulations were conducted in the same thermodynamic conditions as were determined for the tests.

On the basis of the performed simulations it can be stated that the isothermal model of heat exchange provides a satisfactory description of the pressure change in the cylinder. In future scientific research the authors will consider processes of adiabatic and quasi-adiabatic heat exchange in the cylinder with regard to the losses taking place in the real Stirling engine.

Both the theoretical considerations and the workbench tests proved the possibility of adjusting the performance of the Stirling engine by means of changing the working gas mass in the working space and the temperature of the upper heat source (with constant temperature T_c). The workbench tests presented in this work indicate that for nitrogen a temperature increase from 780 K to 910 K for $p = 0.4$ MPa results in electric power growing by over 20 W.

In the case of the model, the temperature increase of the upper heat source was accompanied by an increase in the mean pressure of the working gas in the working space. The theoretical analysis in the present work constitutes a consistent methodology, describing how a dynamic model of the piston-crankshaft system can be integrated with a simulation model.

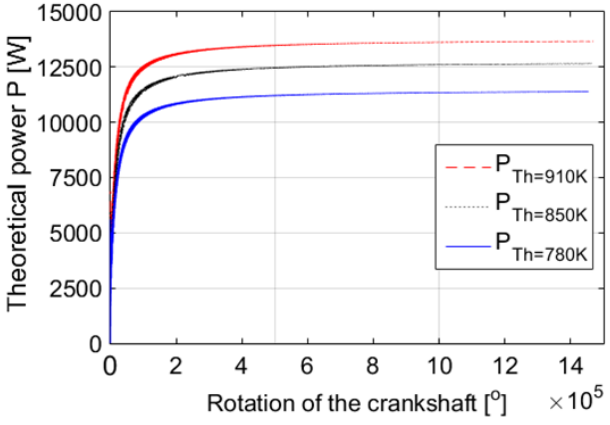

Figure 14: Influence of upper heat source temperature on theoretical power

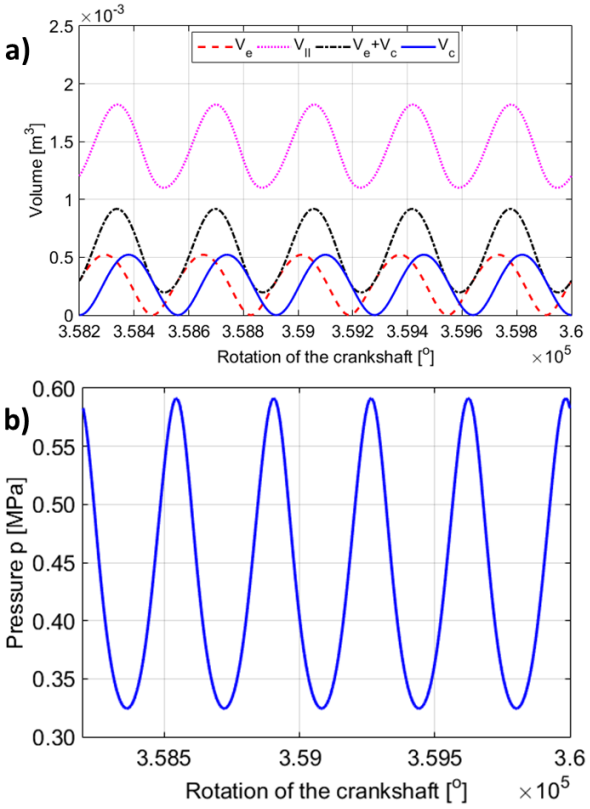

Figure 15: Curves of volume as a function of crankshaft rotation a), open diagram of pressure changes b)

References

[1] EUCO 169/14 Conclusions, accessed 25.09.2015 (23/24 October 2014).
URL http://www.consilium.europa.eu/

[2] B. Knopf, P. Nahmmacher, E. Schmid, The european renewable energy target for 2030–an impact assessment of the electricity sector, Energy policy 85 (2015) 50–60.

[3] A. Calvo-Silvosa, S. I. Antelo, I. Soares, et al., The european low-carbon mix for 2030: The role of renewable energy sources in an environmentally and socially efficient approach, Renewable and Sustainable Energy Reviews 48 (2015) 49–61.

[4] A. Chmielewski, R. Gumiński, S. Radkowski, P. Szulim, Aspekty wsparcia i rozwoju mikrokogeneracji rozproszonej na terenie polski, Rynek energii 5 (114) (2014) 94–101, in Polish.

[5] Directive 2004/8/EC of the European Parliament and of the council of 11 February 2004 on the promotion of cogeneration based on a useful heat demand in the internal energy market and amending Directive 92/42/EC.

[6] J. Milewski, Ł. Szabłowski, J. Kuta, Control strategy for an internal combustion engine fuelled by natural gas operating in distributed generation, Energy Procedia 14 (2012) 1478–1483.

[7] J. Milewski, M. Wołowicz, R. Bernat, L. Szablowski, J. Lewandowski, Variant analysis of the structure and parameters of sofc hybrid systems, in: Applied Mechanics and Materials, Vol. 437, Trans Tech Publ, 2013, pp. 306–312.

[8] A. Chmielewski, R. Gumiński, K. Lubikowski, J. Mączak, P. Szulim, Badania układu mikrokogeneracyjnego z silnikiem stirlinga. część i [research on the micro cogeneration system with stirling engine. part i], Rynek Energii 119 (4) (2015) 42–48, in Polish.

[9] A. Chmielewski, R. Guminski, S. Radkowski, P. Szulim, Experimental research and application possibilities of microcogeneration system with stirling engine, Journal of Power Technologies 95 (5) (2015) 14–22.

[10] A. Chmielewski, R. Gumiński, K. Lubikowski, J. Mączak, P. Szulim, Badania układu mikrokogeneracyjnego z silnikiem stirlinga. Część ii [research on the micro cogeneration system with stirling engine. Part ii], Rynek Energii 120 (5) (2015) 53–60, in Polish.

[11] T. Li, D. Tang, Z. Li, J. Du, T. Zhou, Y. Jia, Development and test of a stirling engine driven by waste gases for the micro-chp system, Applied thermal engineering 33 (2012) 119–123.

[12] C.-H. Cheng, H.-S. Yang, B.-Y. Jhou, Y.-C. Chen, Y.-J. Wang, Dynamic simulation of thermal-lag stirling engines, Applied energy 108 (2013) 466–476.

[13] C.-H. Cheng, H.-S. Yang, L. Keong, Theoretical and experimental study of a 300-w beta-type stirling engine, Energy 59 (2013) 590–599.

[14] M. Reséndiz-Antonio, M. Santillán, On the dynamical vs. thermodynamical performance of a β-type stirling engine, Physica A: Statistical Mechanics and its Applications 409 (2014) 162–174.

[15] G. Xiao, C. Chen, B. Shi, K. Cen, M. Ni, Experimental study on heat transfer of oscillating flow of a tubular stirling engine heater, International Journal of Heat and Mass Transfer 71 (2014) 1–7.

[16] L. Scollo, P. Valdez, S. Santamarina, M. Chini, J. Baron, Twin cylinder alpha stirling engine combined model and prototype redesign, International Journal of Hydrogen Energy 38 (4) (2013) 1988–1996.

[17] C.-H. Cheng, Y.-J. Yu, Dynamic simulation of a beta-type stirling engine with cam-drive mechanism via the combination of the thermodynamic and dynamic models, Renewable energy 36 (2) (2011) 714–725.

[18] C.-H. Cheng, Y.-J. Yu, Combining dynamic and thermodynamic models for dynamic simulation of a beta-type stirling engine with rhombic-drive mechanism, Renewable energy 37 (1) (2012) 161–173.

[19] A. Jankowski, M. Jez, A. Swider, Investigation of non-linear dynamics of crankshaft assembly, Journal of KONES. Internal Combustion Engines 7 (1-2) (2000) 217–227.

[20] M. Jeż, A. Świder, Analiza drgań nieliniowych jednocylindrowego silnika tłokowego, Journal of KONES 8 (3-4) (2001) 98–105, in Polish.

[21] A. Chmielewski, R. Gumiński, S. Radkowski, Chosen properties of a dynamic model of crankshaft assembly with three degrees of freedom, in: Methods and Models in Automation and Robotics (MMAR), 2015 20th International Conference on, IEEE, 2015, pp. 1038–1043.

[22] D. Berchowitz, I. Urieli, Stirling Cycle Engine Analysis, Adam Hilger Ltd, Bristol, 1984.

[23] R. Shoureshi, Analysis and design of stirling engines for waste-heat recovery, Ph.D. thesis, Massachusetts Institute of Technology (June 1981).

[24] G. Walter, Stirling Engines, Oxford University Press, New York, 1980.

[25] D. M. Berchowitz, Stirling cycle engine design and optimisation, Ph.D. thesis (1986).

[26] M. Campos, J. Vargas, J. Ordonez, Thermodynamic optimization of a stirling engine, Energy 44 (1) (2012) 902–910.

[27] S. Toghyani, A. Kasaeian, M. H. Ahmadi, Multi-objective optimization of stirling engine using non-ideal adiabatic method, Energy Conversion and Management 80 (2014) 54–62.

[28] S. Toghyani, A. Kasaeian, S. H. Hashemabadi, M. Salimi, Multi-

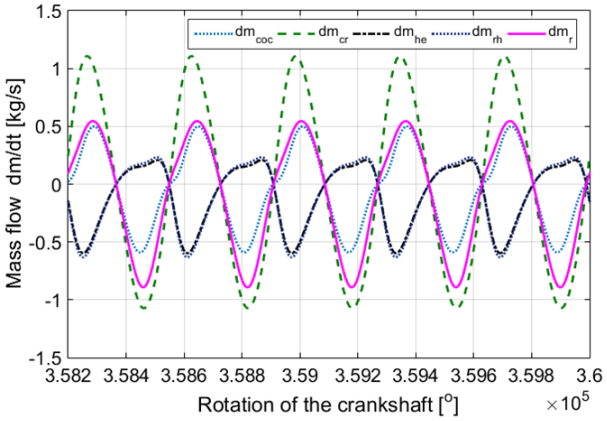

Figure 16: Change in the working gas mass and curves of the model's angular velocity values

objective optimization of gpu3 stirling engine using third order analysis, Energy Conversion and Management 87 (2014) 521–529.
[29] M. Babaelahi, H. Sayyaadi, Simple-ii: A new numerical thermal model for predicting thermal performance of stirling engines, Energy 69 (2014) 873–890.
[30] Y. Timoumi, I. Tlili, S. B. Nasrallah, Performance optimization of stirling engines, Renewable Energy 33 (9) (2008) 2134–2144.
[31] Y. Timoumi, I. Tlili, S. B. Nasrallah, Design and performance optimization of gpu-3 stirling engines, Energy 33 (7) (2008) 1100–1114.
[32] N. Parlak, A. Wagner, M. Elsner, H. S. Soyhan, Thermodynamic analysis of a gamma type stirling engine in non-ideal adiabatic conditions, Renewable Energy 34 (1) (2009) 266–273.
[33] M. Babaelahi, H. Sayyaadi, A new thermal model based on polytropic numerical simulation of stirling engines, Applied Energy 141 (2015) 143–159.
[34] M. H. Ahmadi, M. A. Ahmadi, S. A. Sadatsakkak, M. Feidt, Connectionist intelligent model estimates output power and torque of stirling engine, Renewable and Sustainable Energy Reviews 50 (2015) 871–883.
[35] F. Sala, C. Invernizzi, D. Garcia, M.-A. Gonzalez, J.-I. Prieto, Preliminary design criteria of stirling engines taking into account real gas effects, Applied Thermal Engineering 89 (2015) 978–989.
[36] C. J. Paul, A. Engeda, Modeling a complete stirling engine, Energy 80 (2015) 85–97.
[37] P. Alcan, A. Balin, H. Başlıgil, Fuzzy multicriteria selection among cogeneration systems: a real case application, Energy and Buildings 67 (2013) 624–634.
[38] C.-H. Cheng, H.-S. Yang, Theoretical model for predicting thermodynamic behavior of thermal-lag stirling engine, Energy 49 (2013) 218–228.
[39] J. A. Araoz, M. Salomon, L. Alejo, T. H. Fransson, Non-ideal stirling engine thermodynamic model suitable for the integration into overall energy systems, Applied Thermal Engineering 73 (1) (2014) 205–221.
[40] F. Sala, C. M. Invernizzi, Low temperature stirling engines pressurised with real gas effects, Energy 75 (2014) 225–236.
[41] F. Formosa, G. Despesse, Analytical model for stirling cycle machine design, Energy Conversion and Management 51 (10) (2010) 1855–1863.
[42] A. J. Organ, The regenerator and the Stirling engine, Mechanical Engineering Publications Limited, London, 1997.
[43] S. Żmudzki, Silniki Stirlinga [Stirling Engines], Wydawnictwa Naukowo-Techniczne, Warsaw, 1993.
[44] R. Gheith, F. Aloui, S. B. Nasrallah, Determination of adequate regenerator for a gamma-type stirling engine, Applied Energy 139 (2015) 272–280.

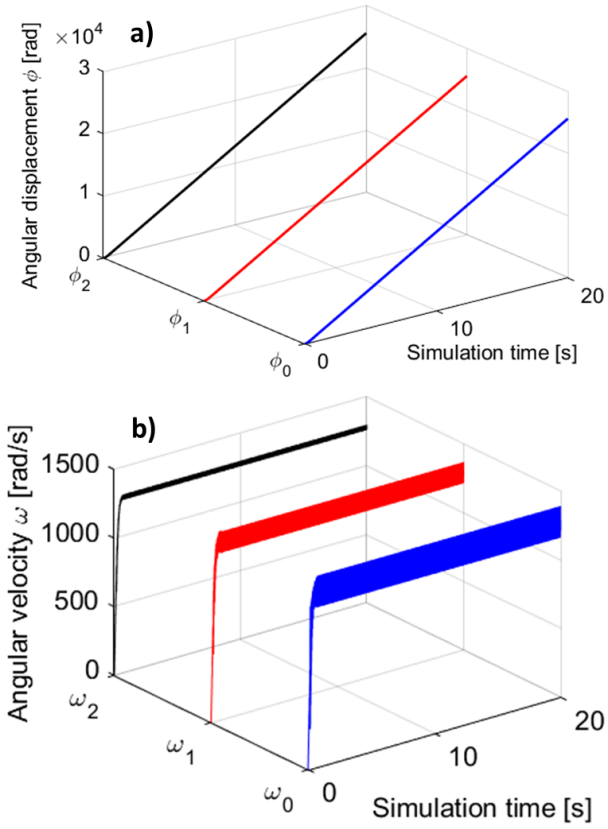

Figure 17: Flow charts of angular displacements a), flow charts of angular velocities b)